JGR Planets

RESEARCH ARTICLE
10.1029/2025JE009027

Cooling History and Evolution Dynamics of Green Glass Beads During Lunar Fire-Fountain Eruptions: Insights From Na, K and Cu Distributions

Xue Su[1], Youxue Zhang[1], Yang Liu[2], and Robert M. Holder[1]

[1]Department of Earth and Environmental Sciences, University of Michigan, Ann Arbor, MI, USA, [2]Jet Propulsion Laboratory, California Institute of Technology, Pasadena, CA, USA

Abstract Volcanic glass beads on the Moon have traditionally been thought to only record volatile loss during pyroclastic eruptions. However, recent discoveries have shown that lunar orange glass beads, representing primitive high-Ti basalts, experienced both outgassing and in-gassing of volatile elements such as Na, K, Cu, and S. In this work, we examine lunar green glass beads from samples 15421 and 15366, representing primitive very-low-Ti basalts, for the distribution of Na, K and Cu using EMP analyses and LA-ICP-MS mapping. It is found that all studied lunar green beads show increased Na, K and Cu concentrations near the bead surfaces, indicative of in-gassing. A quantitative model was developed to simulate the concentration evolution of Na and Cu in individual green glass beads during eruption and cooling. The presence of similar in-gassing diffusion profiles of volatile elements in beads from different eruptions indicates a common behavior of lunar volcanic gas. In addition to volatile in-gassing, LA-ICP-MS mapping of Na and K in one green bead from sample 15366 shows features suggesting collision of melt droplets during the fire-fountain eruption, revealing more details in the dynamic aspects of lunar fire-fountain eruptions. Compared to orange glass beads, the varying boundary conditions of green glass beads during formation may suggest that their eruption plume evolved and dissipated more rapidly, potentially linked to changes in the global lunar atmosphere.

Plain Language Summary Lunar volcanic glass beads, formed during fire-fountain eruptions, preserve key information about lunar volcanism. Traditionally, these beads were thought to primarily record volatile loss. Recent studies on lunar orange glass beads, representing high-Ti lunar basalts, reveal in-gassing of volatile elements such as Na, K, Cu, and S during formation. This suggests that these elements were not only lost to space but also later gained into the beads. However, it is unknown whether in-gassing is a common process during lunar fire-fountain eruptions or is only a local process. In this work, we examined lunar green glass beads, representing very-low-Ti lunar basalts, for the distribution of moderately volatile elements Na, K and Cu. Our results show increased concentrations of these elements near bead surfaces, confirming in-gassing. Additionally, we observed features suggesting collision of melt droplets during eruptions, seen in the Na and K distribution maps of a green bead from sample 15366, shedding more light on the dynamic processes during lunar fire-fountain eruptions. Compared to orange glass beads, the green glass beads may have experienced a different eruption plume that evolved and dissipated more quickly. This may be connected to changes in the global ancient lunar atmosphere.

Key Points:

- Lunar green glass beads are found to have increased Na, K and Cu near the bead surfaces, indicating in-gassing
- By modeling the Na and Cu concentration profiles, the cooling histories of individual lunar green beads are constrained
- Compared to orange beads, the eruption plume during green bead eruptions may have evolved and dissipated more quickly

Supporting Information:

Supporting Information may be found in the online version of this article.

Correspondence to:

X. Su,
xuesu@caltech.edu

Citation:

Su, X., Zhang, Y., Liu, Y., & Holder, R. M. (2025). Cooling history and evolution dynamics of green glass beads during lunar fire-fountain eruptions: Insights from Na, K and Cu distributions. *Journal of Geophysical Research: Planets*, *130*, e2025JE009027. https://doi.org/10.1029/2025JE009027

Received 5 MAR 2025
Accepted 9 JUN 2025

Author Contributions:

Conceptualization: Youxue Zhang, Yang Liu
Data curation: Xue Su, Youxue Zhang
Formal analysis: Xue Su
Funding acquisition: Youxue Zhang, Yang Liu
Investigation: Xue Su, Youxue Zhang, Yang Liu
Methodology: Xue Su, Youxue Zhang, Yang Liu, Robert M. Holder
Project administration: Youxue Zhang
Resources: Youxue Zhang, Yang Liu, Robert M. Holder
Software: Xue Su, Robert M. Holder
Supervision: Youxue Zhang, Yang Liu

© 2025 The Author(s).
This is an open access article under the terms of the Creative Commons Attribution-NonCommercial License, which permits use, distribution and reproduction in any medium, provided the original work is properly cited and is not used for commercial purposes.

1. Introduction

Lunar volcanic glass beads are solidified sub-mm lava droplets that originate from fire-fountain (pyroclastic) eruptions on the Moon (e.g., Delano, 1986; Heiken et al., 1974). During the fire-fountain eruptions, molten lava droplets were ejected at high speeds from the vents into volcanic plumes on the Moon, where they rapidly cooled and solidified to glass beads or other aerodynamic shapes before landing on the surface. Traditional views suggest that these volcanic beads experienced the loss of volatile elements through outgassing (e.g., Saal et al., 2008) from rapid exsolution of volatiles during the ascent of magma. For example, orange glass beads from sample 74220 are found to have lost 99% of the pre-eruptive H_2O compared to melt inclusions hosted in olivine crystals from the same sample (Chen et al., 2015; Hauri et al., 2011, 2015; Ni, Zhang, & Simon 2017, 2019; Saal et al., 2008; Su & Zhang, 2024). Measurements of volatiles (H_2O, F, S and Cl) in a lunar green glass bead from the core to the rim also indicate loss of these elements (Saal et al., 2008). With the advancements of in situ measurements, new observations have provided rich insights into lunar glass beads, which seem to be contradictory to the traditional

Validation: Youxue Zhang, Yang Liu, Robert M. Holder
Visualization: Xue Su
Writing – original draft: Xue Su
Writing – review & editing: Xue Su, Youxue Zhang, Yang Liu, Robert M. Holder

views. For example, recent studies show that in lunar orange volcanic glass beads from sample 74220, concentrations of Na, K and Cu (moderately volatile elements; MVEs) and S (highly volatile element) are elevated near the bead surfaces, forming U-shaped concentration profiles (Su et al., 2023; Su, Zhang, & Liu, 2025). This new discovery indicates that Na, K, Cu and S in the gas phase, which are likely sourced from magma degassing (e.g., Head et al., 2020; Needham & Kring, 2017; Renggli et al., 2017), have in-gassed into the ejected melt droplets as they flew through the eruption plume and cooled down. In addition to eruption-induced plumes, impact events are also capable of producing gas plumes (e.g., Strycker et al., 2013), which could have interacted with glass beads of impact origin. For example, impact glass beads from Apollo 11 are found to have increased Na, K, and P near the rims (Kurat & Keil, 1972), and those from Chang'e−5 also exhibit gradients of K and (or) Na near the bead rims (Pang et al., 2024). The contradiction can be explained by initial outgassing and subsequent in-gassing of volatile elements during the cooling of beads (Su et al., 2023) for volcanic beads and impact beads.

The discovery of in-gassing provides a more comprehensive understanding of the behaviors of volatile elements during the eruption and impact events. It reveals rich details about the history and evolution of lunar beads and the composition of ancient lunar atmosphere, and aids in interpreting the composition of volatile elements in lunar glass. For example, the cooling rates of glass beads can be constrained by fitting the diffusion profiles (Pang et al., 2024; Su et al., 2023; Su, Zhang, & Liu, 2025). Moreover, given that atmospheric components may have been recorded in the beads via in-gassing, investigating in-gassing in lunar glass beads can help re-construct the composition of the lunar atmosphere (Su, Zhang, & Liu, 2025), and reveal additional information about the ancient lunar surface condition (Pang et al., 2024; Su, Zhang, & Liu, 2025).

Despite the importance of in-gassing, whether it is common in lunar glass beads is unclear. Currently, for lunar volcanic glass beads, only orange glass beads in lunar sample 74220 have been investigated for the presence of in-gassing of Na, K, Cu and S (Su et al., 2023; Su, Zhang, & Liu, 2025). In this work, we investigated green glass beads from two other lunar samples, samples 15421 and 15366, for the distribution of Na, K and Cu. Green beads were chosen for this study because they are abundant in lunar samples and represent another important compositional type of lunar volcanic beads. Compared to orange glass beads, green beads have an ultramafic composition but very low Ti contents (<1 wt% TiO_2). We explored whether these elements have in-gassed into lunar green glass beads, similar to their behavior in lunar orange beads, to determine if in-gassing is a common phenomenon in lunar pyroclastic beads from different eruptions. By studying the concentration profiles and distribution of Na, K and Cu, additional information of the cooling history and formation dynamics of the green beads is revealed and discussed.

2. Materials and Methods

In total, six green glass beads from Apollo 15421,8 and two green glass beads from clod 15366,14 were studied in this work. Lunar sample 15421 is the <1 mm fraction of the loose powder broken from large green clods where green clods 15425–15427 were sourced (Lunar Sample Compendium: https://www-curator.jsc.nasa.gov/lunar/lsc/index.cfm). Apollo green clod 15366 is part of the rake sample collected at the rim of Spur crater that is about 40 m away from 15421 (Figure 1). Spherical beads of various sizes were handpicked under a binocular microscope. The picked beads were processed following the procedure in Su et al. (2023), which is briefly described below. After being embedded in epoxy, the beads were polished to reveal the central cross sections. The polished beads were then examined for textural homogeneity using a JEOL JSM-7800FLV Field-Emission Scanning Electron Microscope (FE-SEM) at the University of Michigan. Completely glassy beads without crystallites or bubbles were selected to be measured for major and minor element compositions and mapped for the distributions of Na, K and Cu.

The determination of major and minor element compositions of the green beads was performed using a CAMECA SX-100 Electron Microprobe (EMP) at the University of Michigan. Major and minor elements, including Si, Ti, Al, Cr, Fe, Mn, Mg, Ca, Na and K, were measured using a 10 nA focused beam with an accelerating voltage of 15 kV in focus mode. The counting times and standards used for measurements follow Su et al. (2023) with much improved precision for Na (Table S1 in the repository). Point analysis with a step size of 5–10 μm from rim to rim across the center of the green beads gives concentration profiles of the major and minor elements.

The distributions of Na, K and Cu in the green beads were determined by elemental mapping using Laser-Ablation Inductively Coupled Plasma Mass Spectrometry (LA-ICP-MS) at the University of Michigan following the procedure established in Su et al. (2023). Green beads from samples 15421 and 15366 were

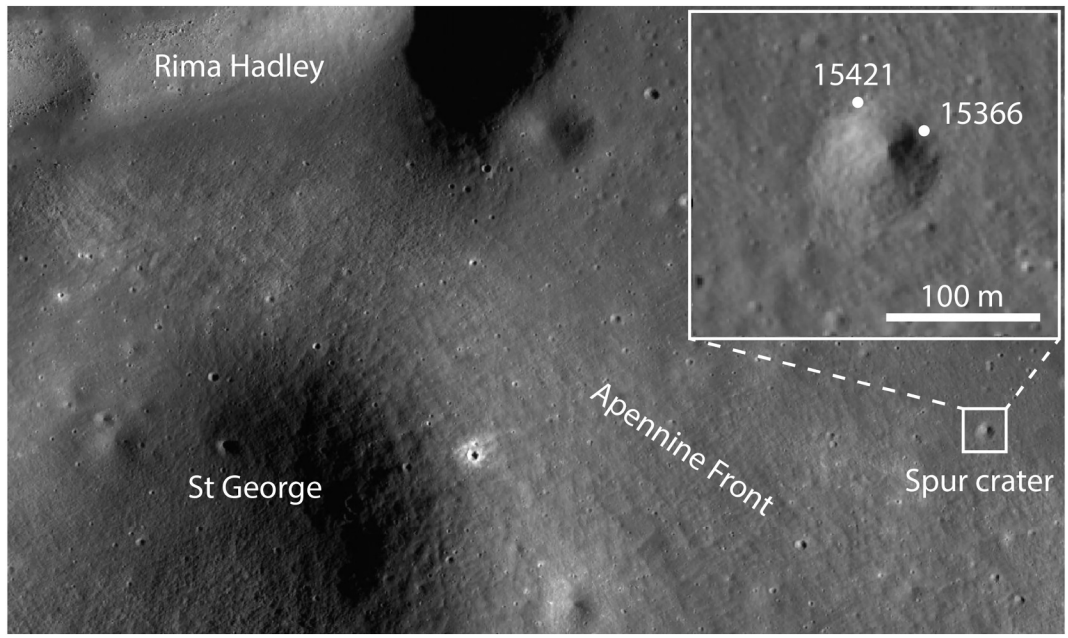

Figure 1. Location of lunar samples 15366 and 15421 near the Spur crater. The base map is from QuickMap (https://quickmap.lroc.asu.edu/).

analyzed in two different sessions. In addition to the elements of interest, Al and/or Fe were included during the analysis as an internal standard. Samples were ablated using an ESI NWR193 excimer laser connected to an Agilent 7900 ICP-MS. For both samples, the fluence was 3.5 J/cm^2 and the beam size was an 8 μm square. Isotope integration times on the ICP-MS and laser scan speeds were set such that the measurement spacing corresponded exactly to the beam size (8 μm). Laser repetition rates were set sufficiently high to minimize signal pulsing, low enough that the depth of ablation should be comparable to the lateral spatial resolution of the maps (~8 μm, assuming ~0.1 μm removal per shot), and an integer factor of the duty cycle to prevent aliasing of the signal if any laser pulsing were still present in the ICP-MS counts (e.g., Van Elteren et al., 2019). For sample 15421, the integration times were 400 ms for ^{23}Na, ^{39}K and ^{63}Cu and 50 ms for ^{27}Al. The scan speed was 4 μm/s and the repetition rate was 40 Hz. For sample 15366, the integration times were 450 ms for ^{23}Na, ^{39}K, and ^{63}Cu and 450 ms for ^{57}Fe with an integration time of 242 ms. The scan speed was 5 μm/s and the repetition rate was 60 Hz. Rasters were constructed by consecutive line-scans. Pre-ablation cleaning shots were performed before each line-scan to remove any surface contamination.

Initial data processing was done with the commercially available software Iolite v4. Baselines were fit and subtracted from the signals, then ^{23}Na, ^{39}K and ^{63}Cu were normalized to either ^{57}Fe or ^{27}Al to correct for drift in instrument sensitivity. FeO and Al_2O_3 are used to correct for drift because their concentrations are relatively homogeneous, with variations <1% relative (Table S2 in the repository). The 2D normalized maps were then converted to 1D radial profiles by concentric ring averaging using the method of Su et al. (2023). The normalized 1D profiles of Na and K were then converted to units of Na_2O and K_2O wt% by scaling to the average EMP Na_2O and K_2O concentrations in the center area of each bead to provide internally consistent data between the analytical methods for diffusion modeling. Using Na and internal standard Al as an example, the conversion can be expressed as: $C_{\mathrm{Na,ICPMS}} = f \times I_{\mathrm{Na/Al,ICPMS}}$, where f is a scaling factor such that $C_{\mathrm{Na,EMP,ctr}} = f \times I_{\mathrm{Na/Al,ICPMS,ctr}}$. For converting Cu/Al count ratios to Cu concentrations, the average Cu concentrations in the center of the studied green beads are assumed to be the same as the Cu concentration from a different 15421 green bead measured by LA-ICP-MS (0.93 ppm; Ni et al., 2019). Hence, Cu concentration in a given green bead m is estimated using $C^{\mathrm{bead}\ m}_{Cu,ctr} = 0.93\ \mathrm{ppm} \times \frac{I^{\mathrm{bead}\ m}_{\frac{Cu}{Al},ctr}}{\left(\sum_{i=1}^{i=n} I^{\mathrm{bead}\ i}_{\frac{Cu}{Al},ctr}\right)/n}$ where n is the number of the green beads. With the acquired center Cu concentrations, the radial profiles of Cu/Al count ratios were converted to Cu concentrations using the same equation, which were then mirrored to form full profiles for modeling.

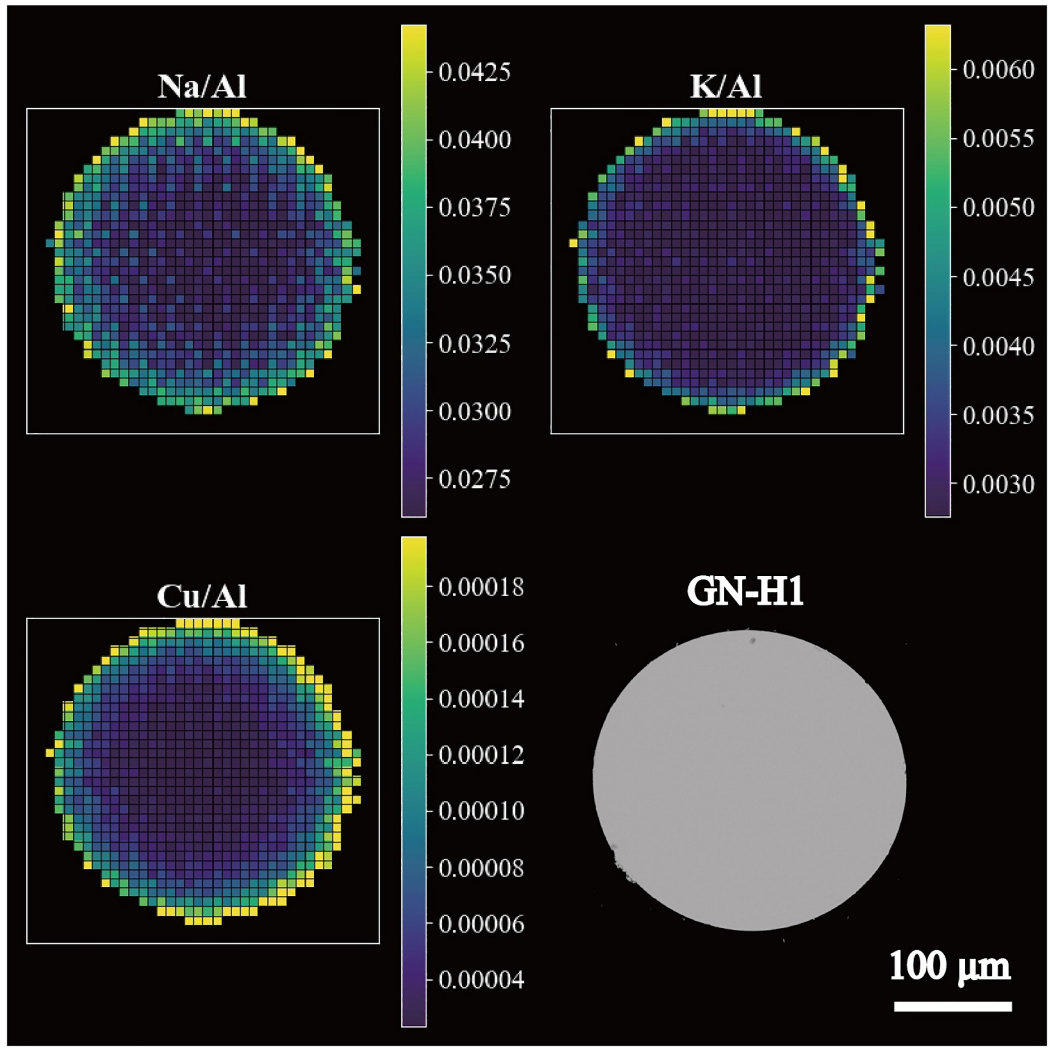

Figure 2. Na/Al, K/Al, Cu/Al maps of a green bead (GN-H1) from sample 15421 from LA-ICP-MS mapping with its backscattered electron (BSE) image. The color bars indicate the counting rate ratios of the measured isotopes. Each pixel represents the size of the square beam (8 × 8 µm).

3. Results

3.1. Green Beads in Lunar Sample 15421

Six green glass beads in sample 15421 were analyzed by EMP and LA-ICP-MS. All beads show increases in Na, K and Cu from the bead centers to the surfaces (Figures 2 and 3). The Na profiles from the two analytical methods are consistent from center to rims (Figure 3), which validates the observation and our method of converting maps to profiles. The bead centers have a Na_2O concentration of 0.11–0.13 wt% and the rims have a Na_2O concentration of 0.15–0.17 wt%, up to ~50% increase relative to the core. K_2O has an average concentration of 0.007–0.012 wt% in the bead centers from EMP, but the trend of K_2O is not discernible due to large relative uncertainties. From LA-ICP-MS, the K_2O trend is clear, which shows that the bead rims have K_2O concentrations of 0.011–0.019 wt% that are up to 40% higher than the centers. The Cu profiles are also U-shaped, with bead centers having a Cu concentration of 0.76–0.94 ppm and bead rims having a Cu concentration of 2.36–6.80 ppm, resulting in a concentration increase of 190%–600% near the bead surfaces. From the profiles and maps, the diffusion distance sequence of the elements is: $x_{Cu} \geq x_{Na} > x_K$. In the discussion section below, the diffusivities of these elements are compared and the occurrence of this sequence is explained. The data from EMP and LA-ICP-MS were reported in Tables S2 and S3 (in the repository), respectively.

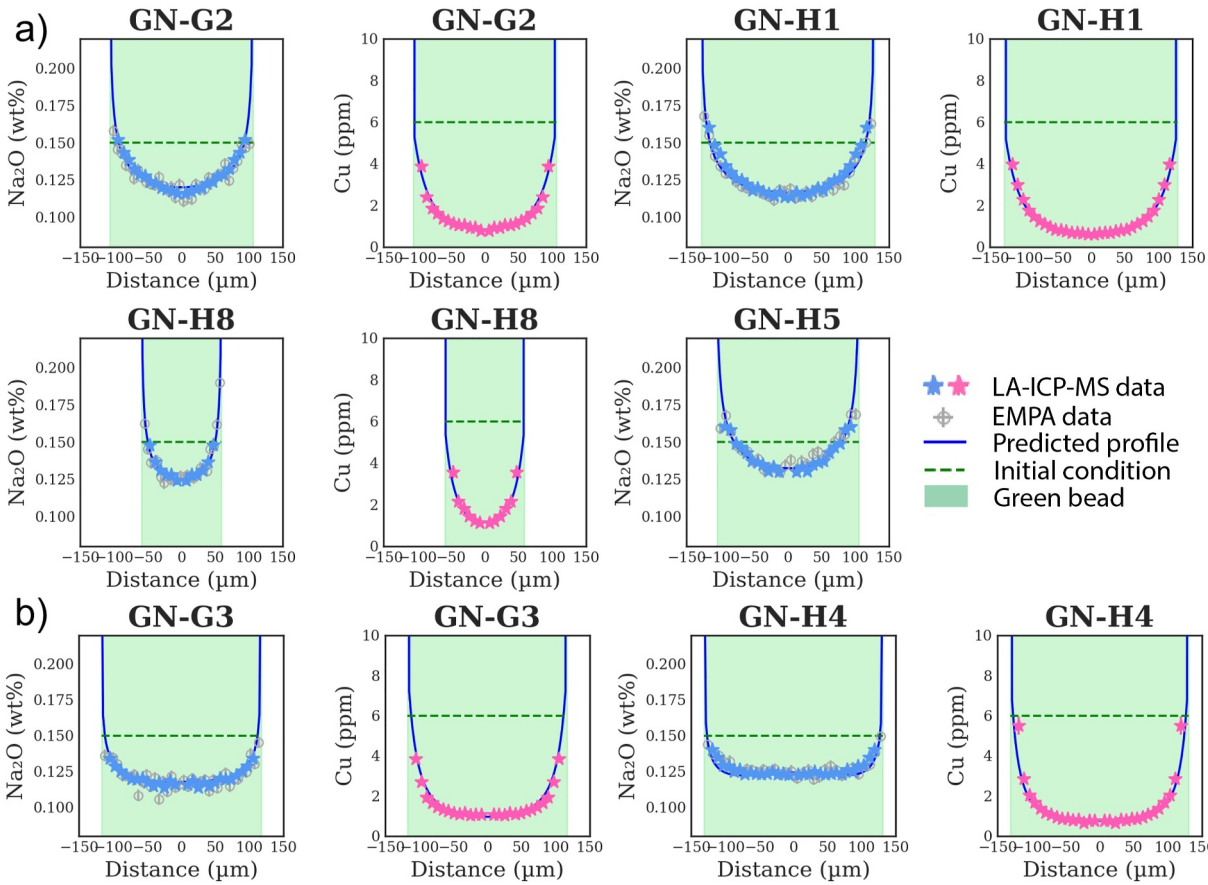

Figure 3. Na and Cu concentration profiles of six green glass beads from sample 15421. Open gray circles represent data from EMP and solid stars represent data from LA-ICP-MS where blue is for Na and pink is for Cu. Solid blue curves represent the predicted concentration profiles from the model in this work. Green dashed lines represent the initial concentrations: 0.15 wt% for Na_2O and 6 ppm for Cu. The green shades represent the green glass beads, where the edges represent the bead surfaces. Panels (a, b) represent beads that are fitted together with the same boundary condition (see main text for details).

3.2. Green Beads in Lunar Sample 15366

Two green glass beads in sample 15366 were analyzed by EMP and LA-ICP-MS. Results can be found in Tables S2 and S3 in the repository. The major and minor element compositions of beads from two lunar samples are very similar (Table S2 in the repository). Among the two studied green beads in sample 15366, one green bead (GNGB3) shows similar in-gassing features of Na, K and Cu as the green beads from sample 15421 (Figure 4a), resulting in U-shaped profiles (Figure 5). The center of this green bead has a Na_2O concentration of 0.12 wt% and the region near the rims has a Na_2O concentration of 0.20 wt%, about 67% higher than the center. The K_2O concentration is 0.01 wt% in the center of the bead, and is 0.023 wt% near the rim, which is up to 130% higher than the center. For Cu, the concentration near the bead surface is near 4.2 ppm and is about 350% higher than the center.

In addition to the in-gassing features, we discovered a new pattern from LA-ICP-MS mapping of Na, K and Cu in the other green bead (GNGB7) in sample 15366. As shown in Figure 4b, the bottom and upper-right of the image show higher concentrations of Na and K than the rest of the bead interior, with a round and slightly elongated shape. These features are most pronounced in the K map (marked as dotted red curves) but are also visible in the Na map. The boundaries between the high-signal-anomaly regions and the rest of the bead are relatively sharp in the K map (a few pixels, ~16 μm). The larger, upper-right anomaly is ~120 μm in diameter. The smaller, bottom anomaly is ~30 μm in diameter. The edge of the larger upper-right anomaly is defined by a distinct anulus of K, ~40% higher than its interior. The Na map exhibits more diffuse gradients across both features. In the Cu map, the anomalous regions are not observable. The causes of the differences in the element maps and the formation of this complex bead are discussed in Section 4.2.

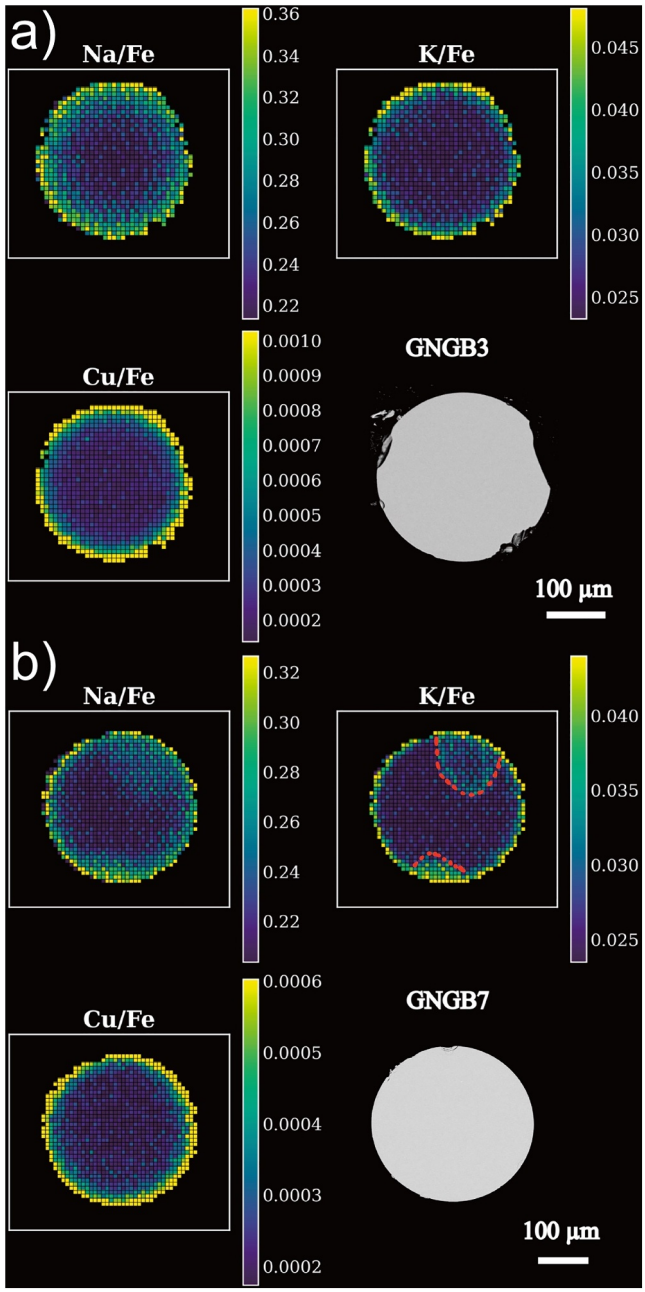

Figure 4. Na/Fe, K/Fe, Cu/Fe maps of two green beads (GNGB3 and GNGB7) from sample 15366 from LA-ICP-MS mapping with the BSE images. The color bars indicate the counting rate ratios of the measured isotopes. Each pixel represents the size of the square beam (8 × 8 µm). The red dotted curves in the K map in (b) mark the boundaries of regions with a characteristic pattern (see the main text).

4. Discussion

4.1. Modeling of Na and Cu Concentration Profiles in Lunar Green Glass Beads

The U-shaped Na and Cu concentration profiles in lunar green beads from samples 15421 and 15366 are modeled by adapting the diffusion model developed by Su et al. (2023). K concentration profiles are not modeled because K diffusivity in basaltic melt is not well known. A first-order estimation of mean K diffusivity in green glass (very-low-Ti lunar basalts) can be made based on the diffusion distances of elements from Figures 2 and 4, in which the Na diffusion distances are about 2 times of the diffusion distances of K in the mapped lunar green glass beads. This observation indicates that the mean D_{Na}/D_K ratio is ≈ 4 in green glass as diffusion distance x is proportional to the square root of the product of diffusivity and time $\sqrt{Dt}$. The estimated first-order mean K diffusivity in green glass (very-low-Ti lunar basalts) agrees well with that in orange glass (high-Ti lunar basalts; Su et al., 2023), which suggests that TiO_2 may not play a significant role in affecting the K diffusivity in lunar basalts.

The diffusion model is capable of simulating concentration changes in the beads during the outgassing and in-gassing processes and constraining the cooling time scales (or cooling rates) of the beads as an output. The model details including assumptions are summarized below. Given the spherical shape of the beads, the diffusion equation can be expressed as follows:

$$\frac{\partial(rC)}{\partial t} = D\frac{\partial^2(rC)}{\partial r^2}, \quad (1)$$

where r is radial distance in meter (m), and C is Na_2O (in wt%) or Cu concentration (in parts per million by weight, ppm), t is time in second (s), and D is diffusivity of Na or Cu in m^2/s. For Na, we use the experimentally determined diffusivity in alkali basalt from Lowry et al. (1982), which shows negligible dependence on melt composition from basalt to andesite. The expression of the Na diffusivity is: $D_{Na} = \exp(-9.251-19628/T)$ where T is the temperature in Kelvin (K). Cu diffusivity in basaltic melt was first constrained by Ni and Zhang (2016). The melt composition effect on Cu diffusivity was explored in Ni, Zhang, and Guan (2017) and Zhang and Gan (2022), who found the dependence of Cu diffusivity on the mole fraction of Si, Al and H in the melt. Using their general equation for Cu diffusivity and the major element composition in the center of the green beads determined by EMP in this study (Table S2 in the repository), the expression of Cu diffusivity used in the model is: $D_{Cu} = \exp(-15.2-9{,}355/T)$. H is assumed to be negligible in estimating the Cu diffusivity in green beads because of its low H_2O concentration at tens of ppm level (Saal et al., 2008). These expressions predict that the diffusivity of Cu should be slightly higher than that of Na at temperature < 1,725 K, consistent with the qualitative observations of this study.

At a lunar fire-fountain eruption, droplets of melt formed at fragmentation in the magma conduit, which later erupted to the surface and quenched to glass beads. Assuming fragmentation is the initial stage where a melt droplet with radius a (in m) has a homogenous composition, the initial condition is:

$$C|_{0\le r\le a} = C_0 \text{ (at } t=0). \quad (2)$$

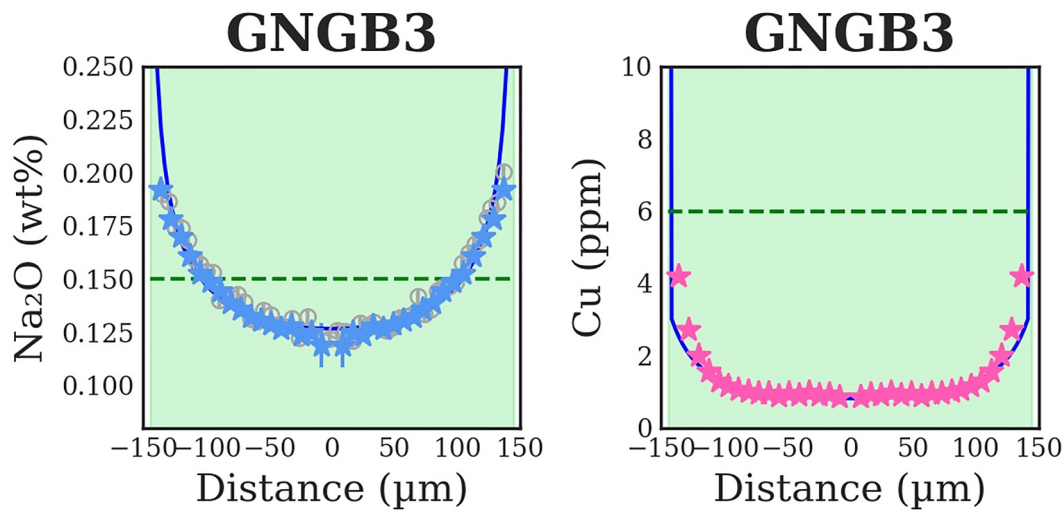

Figure 5. Na and Cu concentration profiles of a green glass bead (GNGB3) from sample 15366. Other symbols are the same as Figure 3.

For lunar orange glass beads, initial concentrations of moderately volatile elements before fragmentation are assumed to be the same as those in the olivine-hosted melt inclusions, which represent pre-eruptive contents found in the same lunar sample. For instance, initial concentrations of 0.35 wt% for Na_2O and 8 ppm for Cu are used to model the Na_2O and Cu profiles in orange glass beads (Su et al., 2023), based on the Na_2O and Cu contents in olivine-hosted melt inclusions (Chen et al., 2015; Hauri et al., 2011; Ni et al., 2019; Su & Zhang, 2024) associated with orange glass beads. However, for lunar samples with lunar green glass beads, no melt inclusions have been found, and therefore no data are available regarding the initial concentrations of elements in green glass beads. Compared to orange glass, green glass has much lower concentrations of incompatible elements such as rare earth elements (REEs; e.g., Shearer & Papike, 1993). Hence, the initial concentrations of Na_2O and Cu used in orange glass bead modeling may be too high for modeling the Na_2O and Cu profiles in green glass beads. Here, we tackle this problem by making an initial assumption that green beads have a similar degree of loss of Na_2O and Cu compared to that of orange beads. As a result, an initial concentration of 0.15 wt% for Na_2O and 6 ppm for Cu were estimated and used in modeling the green beads. In the Supporting Information S1, we explored how the selection of initial Na_2O and Cu within a reasonable range (Na_2O from 0.13 to 0.20 wt% and Cu from 4 to 8 ppm) affects the model results. It is demonstrated that by adjusting the initial Na_2O and the initial Cu concentrations within the ranges above, the cooling time scales of the green beads are varied within 36%. Hence, varying the initial concentrations within a reasonable range does not significantly affect the model results. This may be explained by the fast diffusivity of Na and Cu, and the fast boundary reaction (in equilibrium) between the gas and melt. The initial temperature at fragmentation is assumed to be 1,680 K using the average liquidus temperature of green beads from Apollo 15, which is slightly higher than that of the orange beads (Delano, 1990).

At the glass bead surface, fast equilibrium with the ambient atmosphere is assumed during the cooling of the beads. Quantitative vaporization experiments on Apollo 12 lunar samples have shown that the equilibrium partial pressure of Na exhibits a clear temperature dependence, which increases at higher temperatures (De Maria et al., 1971). The difference between the equilibrium partial pressure and ambient partial pressure of an element in the atmosphere decides whether it is outflux or influx of the element at the glass bead surface-atmosphere interface (Su et al., 2023), which is ultimately controlled by temperature. Su et al. (2023) proposed that the boundary condition can be expressed as

$$C_e = a_0 \times e^{\frac{b_0}{T}} (\text{at } r = a), \tag{3}$$

where C_e is the concentration of Na_2O and Cu at the surface of a bead, and a_0 and b_0 are two free fitting parameters in the model. The detailed rationale of the boundary condition is justified in Su et al. (2023). The boundary condition implies that the bead surface Na_2O and Cu concentrations decrease with increasing temperature

Table 1
Fitting Results of Six Green Beads From Sample 15421

a_0 (Na_2O) (wt%)	0.0308(17)	b_0 (Na_2O) (K)	1,877(47)
a_0 (Cu) (ppm)	0.0000322(583)	b_0 (Cu) (K)	10,681(1,519)
Bead #	Diameter (μm)	τ (s)	Element
GN-G2	212	285(115)	Na (E + L), Cu (L)
GN-H1	257	310(129)	Na (E + L), Cu (L)
GN-H8	118	127(50)	Na (E + L), Cu (L)
GN-H5	210	779(316)	Na (E + L)
Total MSWD	1.23		
a_0 (Na_2O) (wt%)	0.0518(30)	b_0 (Na_2O) (K)	1,242(84)
a_0 (Cu) (ppm)	0.00538(106)	b_0 (Cu) (K)	6,498(253)
Bead #	Diameter (μm)	τ (s)	Element
GN-G3	234	70(3)	Na (E + L), Cu (L)
GN-H4	262	47(2)	Na (E + L), Cu (L)
Total MSWD	1.76		

Note. In the element column, E represents the data from EMP, and L represents data from LA-ICP-MS. The value in parentheses is one standard deviation on the last digit.

(outgassing) and increase with decreasing temperature (in-gassing). Consequently, starting at the fragmentation, due to the high temperatures, volatile elements including Na and Cu in melt droplets began to release to the environment in the vapor phase, sustaining the ambient local atmosphere. Outgassing continued as the melt droplets erupted. The melt droplets were cooling as they flew through the local atmosphere away from the vent. When the temperature of the melt droplets decreased to a certain point, in-gassing became dominant and gas molecules carrying Na, Cu and other volatile elements began to diffuse back into the melt droplets. The cooling of the melt droplets during the eruption is approximated as asymptotic cooling: $T = \frac{T_0}{1+\frac{t}{\tau}}$ (Zhang, 2008), where τ represents the cooling time scale. The cooling rate q at a certain temperature T can be calculated as $q = -\mathrm{d}T/\mathrm{d}t = T^2/\tau T_0$.

With the diffusion equation, initial condition and boundary condition (Equations 1–3), and measured Na and Cu concentration profiles across green beads, unknown parameters a_0 and b_0 for Na and Cu, and cooling time scales of individual green beads can be fitted. Calculations are terminated at the glass transition temperature of green glass beads at 883 K (Arndt et al., 1984). When fitting the Na_2O and Cu concentration profiles of different beads, Su et al. (2023) assumed that: (a) the cooling time scale of a certain bead should be independent of which elements are being investigated, and (b) the a_0 and b_0 values of an element should remain consistent across different beads. In this work, when we initially fitted measured Na_2O and Cu concentration profiles of all green beads together, it was found that the fitting performance varies from bead to bead. For some green beads, modeled profiles of both Na and Cu match well with the measured profiles; for other green beads, modeled profiles can only reproduce the measured Cu profiles (because Cu concentration variation is much larger), leaving Na_2O profiles poorly fitted. This result means that the boundary condition may vary from bead to bead with different a_0–b_0 pairs of Na and Cu, which may be the result of a heterogenous atmosphere interacting with beads or different pulses of eruption. Based on this finding and the performance of beads, we categorize the green beads in sample 15421 into two groups and fit their Na_2O and Cu concentration profiles together within each group to obtain separate boundary conditions (i.e., a_0–b_0 pairs for Na and Cu). The Na_2O and Cu concentration profiles of the green bead in sample 15366 is fitted separately as well because it is from a different location. With this treatment, all measured Na_2O and Cu concentration profiles of green beads in this work can be fitted well with a mean squared weighted deviation (MSWD) close to 1 (e.g., Wendt & Carl, 1991). Tables 1 and 2 present the fitting results of green beads from sample 15421 and 15366, respectively, and the fitting profiles are shown in Figures 3 and 5 as blue solid curves.

Based on the constrained boundary conditions of the beads, we plotted the surface concentration evolution (C_e) of Na and Cu with temperature to probe the composition information of the atmosphere in Figure 6. The figure shows that the green bead from sample 15366 was in contact with the eruption plume with more Na and less Cu than the eruption plume associated with green beads in sample 15421. Even within beads from the same sample (15421), the boundary conditions are not the same. For example, the plume that green beads GN-G3 and GN-H4 were in contact with has less Na and more Cu than the plume of other green beads in the same lunar sample experienced. There are two possibilities to explain this observation. One possibility is that these beads may have been erupted at a different time from the other four beads in the same sample when the chemical composition of the local eruption plume had evolved. The evolution of the eruption plume during a lunar pyroclastic event has been inferred from analyses of surface sublimates on volcanic beads (Williams et al., 2025). Given that the major element compositions of green beads GN-G3 and GN-H4 are nearly the same as other green beads in sample 15421 (Table S2 in the repository), the time interval between the pulses may be short such that the composition of the magma does not evolve significantly. A second possibility is that beads GN-G3 and GN-H4 were ejected from the vent at much lower launch angles compared to the other four beads in sample 15421. Trajectory calculations of volcanic ejecta indicate that the maximum

Table 2
Fitting Results of a Green Bead From Sample 15366

a_0 (Na_2O) (wt%)	0.0172(11)	b_0 (Na_2O) (K)	3,017(142)
a_0 (Cu) (ppm)	0.0176(158)	b_0 (Cu) (K)	4,620(714)
bead #	Diameter (μm)	τ (s)	Element
GNGB3	289	152(106)	Na (E + L), Cu (L)
Total MSWD	1.59		

Note. Notations are the same as Table 1.

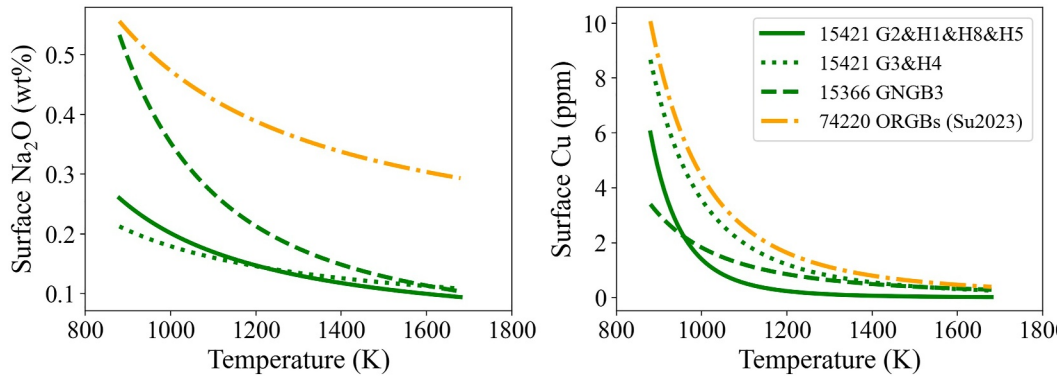

Figure 6. Evolution of surface Na_2O (left) and Cu (right) concentrations of the green (this work; Tables 1 and 2) and orange glass beads (Su et al., 2023) with cooling.

horizontal travel distance occurs at a 45° launch angle, but material can reach the same landing site from both lower and higher angles (Saunderson, 2008). The significantly shorter cooling time scales of green beads GN-G3 and GN-H4 suggest that they encountered the colder eruption plume edge earlier, consistent with a lower launch angle. In contrast, the longer cooling time scales of the other four green beads in sample 15421 imply a higher launch angle, resulting in extended exposure to the hotter central region of the plume before quenching at the plume edge. The different boundary conditions of these green beads indicate that the eruption plume may have less Na and more Cu near the edge. Nevertheless, this result reveals the dynamic nature of the local eruption plume (atmosphere) during a lunar fire-fountain eruption, which evolved quickly and may have a heterogeneous or time-dependent composition. On the other hand, at the initial temperature (T_0 = 1,680 K; Figure 6), the model shows that the surface Na_2O and Cu concentrations of all modeled green glass beads are nearly identical. It indicates that at fragmentation when melt droplets just formed, they had a similar level of surface equilibrium Na_2O and Cu concentrations. This is physically meaningful and as expected because the ambient gas pressures in the magma conduit are supposed to be more stable and consistent compared to heterogeneous and changing gas pressures in the eruption plume. Compared to the green glass beads, orange beads have much higher surface Na_2O and slightly higher Cu concentrations (Figure 6). The abundant Na-carrying gas molecules in the eruption plume of orange glass bead eruption help maintain the Na content in orange glass beads and facilitate the formation of surface Na-rich condensates (Liu & Ma, 2022; Ma & Liu, 2019). In contrast, there are no clear Na-rich condensates on the surface of lunar green glass beads (Liu et al., 2020; Liu & Ma, 2024). This observation is consistent with the modeled surface Na_2O of green beads in this work, which may be too low to be saturated for forming condensates.

The cooling time scales (τ) constrained for individual lunar green beads ranged from 47 to 779 s, corresponding to cooling rates of 2–36 K/s at the initial stage (T_0 = 1,680 K) and 1–13 K/s at 1,000 K. Previous studies have estimated the cooling rates of lunar green beads. For instance, Arndt et al. (1984) determined the critical cooling rate (the minimum rate at which the melt quenched to glass without crystallization) of lunar green glass to be 1 K/s, aligning with the lower limit of our findings. Thermal expansion experiments of Arndt and Rombach (1976) in lunar green glass indicate a cooling rate of 2–20 K/s. From theoretical calculations, it is suggested that lunar green glass has a cooling rate of about 9 K/s (Birnie III & Dyar, 1986). These estimates are consistent with our constrained values for individual green glass beads. In comparing with lunar orange glass beads, the values are also found to be similar (Arndt & Von Engelhardt, 1987; Hui et al., 2018; Ni, Zhang, Simon, & Gagnon, 2017; Su et al., 2023). This indicates a similar surface thermal environment during orange and green bead eruptions, probably because of a similar eruption style and cooling mode.

4.2. Discovery of a Complex Bead Formed From Melt Droplet Collisions

In addition to the discovery of in-gassing of Na, K and Cu in lunar green glass beads, features suggesting collision of melt droplets during the fire-fountain eruption were also observed from LA-ICP-MS in one green bead from lunar sample 15366 (Figure 4b). The signal anomaly in the upper right and bottom regions with a round shape is the most distinct in the K map exhibiting a clear boundary. This pattern is less discernible in the Na map and is not observable in the Cu map. The cause of the different patterns observed in different element maps is likely due to

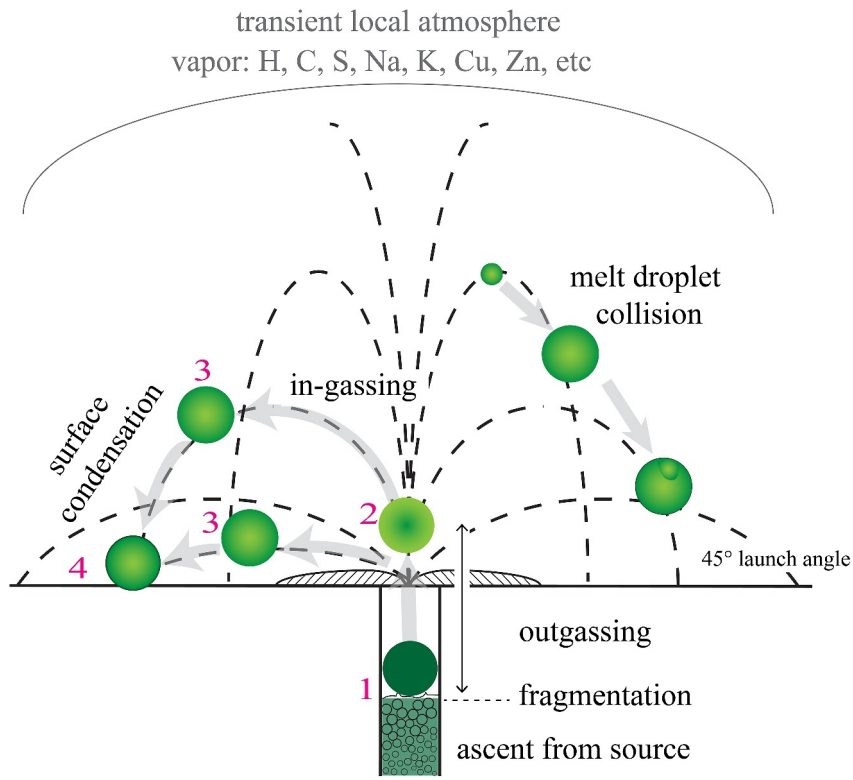

Figure 7. Illustration showing the formation of the lunar green glass beads during a fire-fountain eruption. The left side of the figure depicts the processes that occurred during the formation of the beads that eventually lead to the volatile concentration distribution observed in this work with high and low launch angles from the vent. The shade of green colors represents the abundance of volatile elements in the beads where deeper green means higher concentration and lighter green means lower concentration. The right side of the figure shows the collision of two melt droplets. Not to scale: for example, the bead sizes after fragmentation are drawn much larger than to scale for clarity.

their different diffusivities. As discussed in Section 4.1, the diffusivity sequence among volatile elements Na, K and Cu is: $D_{Cu} \geq D_{Na} > D_K$ in basaltic melt. The high diffusivity of Cu in green glass has resulted in the erasure of the pattern in the Cu map. Conversely, due to the low diffusivity, the pattern remains well-preserved in the K map. Since there is little major-element heterogeneity among different regions, the pattern is indistinguishable in the BSE image (Figure 4b).

From the round shapes of the regions with high Na and K signals, we hypothesize that the whole bead may have formed from the collision of three melt droplets: A large one collided with two smaller ones. Each of those three melt droplets forming this complex bead is also found to be zoned due to outgassing and in-gassing. For the droplet represented by the upper-right anomaly, K is zoned with higher counts near the rim and lower counts in the center, resembling the same in-gassing pattern observed at the rim of the aggregate bead; we interpret this to have been the result of prior outgassing and in-gassing of the sub-droplets before collision. The rim of this droplet has a higher K than its interior but not as high as the host melt droplet because in-gassing of the host droplet continued during further cooling after collision. Na zonation is not observed in the smaller melt droplets because Na has higher diffusivity than K and therefore the pattern has been homogenized with an indistinct boundary. For the host melt droplet, in-gassing of Na, K and Cu results in a higher signal rim than the interior, like other green beads. For the droplet represented by the bottom anomaly, it has higher Na and K signals than the outer host melt droplet with no noticeable zonation even in the K map. Due to its small size (~30 μm across), it is likely that the space resolution from an 8 × 8 μm square laser beam is not small enough to distinguish it.

Figure 7 depicts the formation of lunar green glass beads during a fire-fountain eruption. The left side illustrates the sequence of the processes from fragmentation, outgassing, in-gassing to surface condensation that leads to the current observations on the beads. Deeper green shades indicate a higher concentration of volatile elements in the beads, and vice versa for lighter green colors. The right side shows the formation of the complex bead due to the

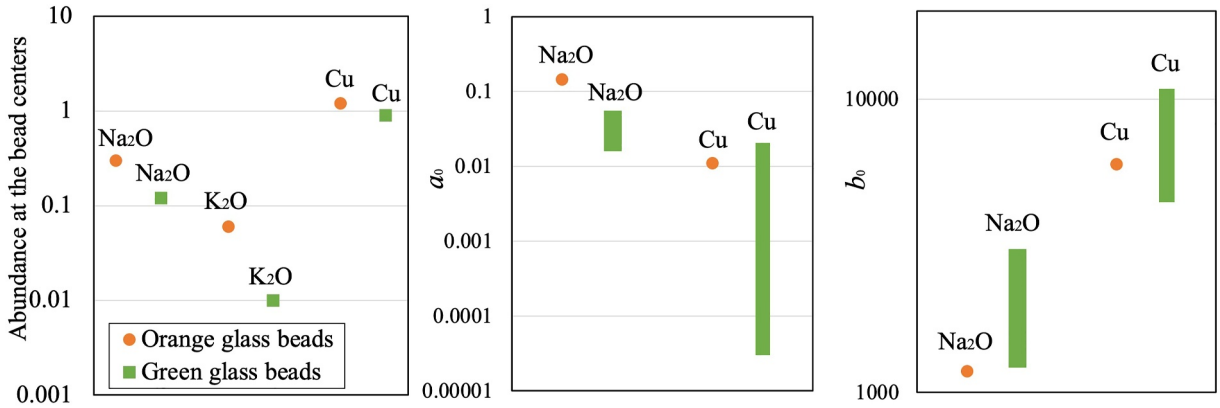

Figure 8. Left: Comparison of Na_2O, K_2O and Cu abundances in the centers of orange and green glass beads. Na_2O and K_2O data are in wt% and are from this work, and Cu data are in ppm and are from Ni et al. (2019). Middle: Comparison of fitted a_0 values for Na_2O and Cu of orange and green glass beads. Right: Comparison of fitted b_0 values for Na_2O and Cu of orange and green glass beads. The fitted a_0 and b_0 data of orange beads are from Su et al. (2023), and those of green beads are from this work.

collision between melt droplets while maintaining the features from outgassing and in-gassing. The discovery of the complex bead formed from melt droplet collisions highlights the dynamics of lunar fire-fountain eruptions and has the potential to reveal further details about the processes involved in these events.

4.3. Comparison of In-Gassing in Lunar Green and Orange Beads, and Implications

The observation of elevated signals of Na, K and Cu near green bead surfaces compared to the centers in samples 15421 and 15366 indicates the presence of in-gassing during the formation in the fire-fountain eruptions. This observation is consistent with the discovery of in-gassing of Na, K, Cu, and S in orange glass beads from lunar sample 74220 (Su et al., 2023; Su, Zhang, & Liu, 2025). In-gassing of Na and K has been reported in impact glass beads from Chang'e−5 (Pang et al., 2024) and Apollo 11 samples (Kurat & Keil, 1972). However, glass beads of impact origin are generally more complicated than those of volcanic origin because of more complex and variable starting materials, thermal histories, inhomogeneity, and potential changes in redox conditions experienced by impact beads (e.g., Pang et al., 2024). Hence, in the discussion below, we focus on comparing the in-gassing of volatile elements among lunar volcanic glass beads.

Compared with orange glass beads, green glass beads have lower volatile contents (Figure 8, left panel). In addition, the modeled surface concentrations of Na_2O and Cu were also lower in green glass beads than in orange glass beads (Figure 6). The results reflect the amount of Na and Cu in the local eruption plume: higher Na and Cu pressures during the orange bead eruption and lower Na and Cu pressures during the green bead eruption (Figure 6). The same conclusion is expected to hold for K even though no detailed model is possible. The comparisons of the fitted a_0 and b_0 values for Na_2O and Cu of orange and green glass beads are plotted in Figure 8. It is found that the fitted a_0-b_0 pairs of Na and Cu in orange beads are robust from bead to bead, while the fitted a_0-b_0 pairs of Na and Cu in green beads are quite variable (Table 1; Figures 6 and 8). One possibility is that the eruption plume may have evolved quickly during the green bead eruption so that the boundary conditions were changing among the green beads.

In addition to the difference in Na_2O and Cu diffusion profiles, orange and green glass beads also show different levels of enrichment of volatile elements on the surface in the form of surface coating and minerals. Surface coating and minerals have been interpreted to result from condensed volcanic vapor, where lunar orange beads are found to have more widespread and stronger volatile enrichments than green glass beads. For example, wide-occurring euhedral μm-sized Zn-Na-S-Cl and Na-K-S minerals have been directly observed on the surface of orange glass beads (Liu & Ma, 2022; Ma & Liu, 2019). On the surface of green beads, Zn-S phases have been found, but they are more amorphous and much smaller than the vapor condensates on orange beads (Liu et al., 2020; Liu & Ma, 2024; Ross et al., 2011). Depth profiling on both orange and green beads shows that the bead surfaces have enrichments of Na, K, Zn, S and F in the coating, but the count rates at the peaks are much lower in green beads compared with orange beads (Meyer et al., 1975). These observations further show that the

eruption plume during green glass bead eruptions may be thinner compared to the eruption plume during orange glass bead eruptions.

Studies on the global transient lunar atmosphere sourced from mare basalt emplacement suggest that the global atmospheric surface pressure reached the maximum when mare volcanism peaked, during 3.4–3.8 Ga with a maximum flux at ∼3.6 Ga (Head et al., 2020, 2023). Considering that the age is about 3.54–3.66 Ga for orange glass (Alexander et al., 1978; Huneke, 1978; Huneke et al., 1973) and 3.35–3.41 Ga for green glass (Podosek & Huneke, 1973; Spangler et al., 1984), it is possible that the stable, relatively high Na and Cu local eruption plume of orange beads was buffered and maintained by a much larger-scale atmosphere due to the concurrent peak of mare volcanism. At the time of green bead eruptions, because mare volcanism declined, the larger-scale atmosphere became thinner and was only able to maintain the local eruption plume for a relatively short time. Hence, the eruption plume during green bead eruptions may evolve and dissipate quickly. The interaction between the global atmosphere and local eruption plumes and the quantification of global and local atmospheric pressures need further investigations, but the difference between the plumes from orange and green glass bead eruptions is undoubtful.

The occurrence of similar in-gassing diffusion profiles of Na, K and Cu in different pyroclastic beads from different eruptions implies that it is a common behavior of volatile elements in lunar volcanic gas. The behavior of outgassing and in-gassing is mainly controlled by temperature: Outgassing prevails at higher temperatures, while in-gassing becomes dominant at lower temperatures. Generally, for in-gassing to occur, there are a few prerequisites: (a) The diffusivity of the element of interest needs to be high enough to produce measurable diffusion distance under the temperature range and duration of the event, and (b) the partial pressure of the vapor phase carrying the element of interest needs to be higher than the equilibrium partial pressure for the element to migrate from vapor to melt. Consequently, it is reasonable to predict that in-gassing can occur in other lunar volcanic glass beads. Lunar impact glass beads could also have experienced in-gassing as the immense energy from the collision could cause partial melting and release of volatile elements to temporarily sustain a local atmosphere. For instance, impact beads from Apollo 11 and Chang'e−5 are found to have higher Na and K concentrations near the rims than the bead interiors (Kurat & Keil, 1972; Pang et al., 2024).

There are many important implications of the interactions between melt droplets and ambient atmosphere in the form of outgassing and in-gassing. Specifically, key information such as the composition, temperature and pressure of the local transient atmosphere, the depletion or enrichment of volatile elements in glass beads, the cooling history of glass beads, and possible other processes occurred in the atmosphere has been recorded. The hypothesis of a local atmosphere containing Na, K, Cu and S in the gas phase with relatively high partial pressures is supported by the discovery of their in-gassing profiles in the glass beads. As shown in Section 4.1, cooling history information can be extracted from modeling the diffusion profiles of the beads. Additionally, Su, Zhang, and Liu (2025) demonstrated that in-gassing of S can significantly affect the ^{33}S isotopic composition in lunar orange beads, where the observed ^{33}S anomaly in the orange glass beads (Dottin et al., 2023) is attributed to the input of atmospheric S with a distinct ^{33}S signature. These findings underscore the importance of lunar glass beads as a unique window into the physical and chemical conditions of the ambient environment during their formation.

5. Conclusions

EMP analyses and LA-ICP-MS mapping on the moderately volatile element Na, K and Cu distributions in lunar green glass beads from samples 15421 and 15366 reveal that these elements have elevated concentrations near bead surfaces compared to the centers, indicating in-gassing. The similar observation of in-gassing of the moderately volatile elements Na, K and Cu in lunar green and orange beads, which represent very-low-Ti and high Ti lunar basalts, suggests that in-gassing was not a local feature but a common behavior of these elements in the lunar atmosphere during fire-fountain eruptions. A quantitative model is used to fit the measured Na and Cu profiles and constrain the cooling histories of the individual green beads. Based on the model, the cooling time scales of the green beads ranged from 47 to 779 s, corresponding to cooling rates of 2–36 K/s at the initial stage (T_0 = 1,680 K) and 1–13 K/s at 1,000 K. This estimation is consistent with previous studies on the cooling rates of lunar green glass. In addition to in-gassing, one green bead from lunar sample 15366 shows features suggesting the collision of melt droplets during the fire-fountain eruption. According to the K distribution map from LA-ICP-MS, the merged melt droplets exhibit a distinct boundary and are zoned as well due to the outgassing and in-

gassing processes. By comparing to orange beads, the eruption plume during green bead eruptions may have evolved and dissipated more quickly based on the constrained boundary conditions.

Data Availability Statement

Data in this work (including Tables S1–S3 with EMPA data and LA-ICP-MS mapping data, BSE images of all beads and python code for modeling) are available through the University of Michigan's open-access digital repository service and can be found at Su, Zhang, Liu, et al. (2025).

Acknowledgments
We thank NASA CAPTEM for providing the lunar samples. We are grateful to Editor Jean-Pierre Williams for handling the manuscript, and to reviewers Steve Parman and Jim Van Orman for providing constructive and insightful comments. This research was supported by NASA Grant 80NSSC23K1297 and JPL's Strategic University Research Partnerships (SURP) program. YL's contribution was conducted at the Jet Propulsion Laboratory, California Institute of Technology, under a prime contract with the NASA Administration (80NM0018D0004). The CAMECA SX-100 Electron Microprobe used in this work was purchased using NSF Grant EAR-9911352.

References

Alexander, E., Coscio, M., Dragon, J., & Saito, K. (1978). ^{40}Ar-^{39}Ar studies of glasses from lunar soils (abstract). *Proceedings of the Lunar and Planetary Science Conference* (Vol. 9, 7–9).

Arndt, J., Engelhardt, W., Gonzalez-Cabeza, I., & Meier, B. (1984). Formation of Apollo 15 green glass beads. *Journal of Geophysical Research*, *89*(S01), C225–C232. https://doi.org/10.1029/JB089iS01p0C225

Arndt, J., & Rombach, N. (1976). Derivation of the thermal history of tektites and lunar glasses from their thermal expansion characteristics. *Proceedings of the Lunar and Planetary Science Conference* (Vol. 7, 1123–1141).

Arndt, J., & Von Engelhardt, W. (1987). Formation of Apollo 17 orange and black glass beads. *Journal of Geophysical Research*, *92*(B4), E372–E376. https://doi.org/10.1029/JB092iB04p0E372

Birnie III, D. P., & Dyar, M. D. (1986). Cooling rate calculations for silicate glasses. *Journal of Geophysical Research*, *91*(B4), 509–513. https://doi.org/10.1029/JB091iB04p0D509

Chen, Y., Zhang, Y., Liu, Y., Guan, Y., Eiler, J., & Stolper, E. M. (2015). Water, fluorine, and sulfur concentrations in the lunar mantle. *Earth and Planetary Science Letters*, *427*, 37–46. https://doi.org/10.1016/j.epsl.2015.06.046

Delano, J. W. (1986). Pristine lunar glasses: Criteria, data, and implications. *Journal of Geophysical Research*, *91*(B4), 201–213. https://doi.org/10.1029/JB091iB04p0D201

Delano, J. W. (1990). Buoyancy-driven melt segregation in the earth's moon. I-Numerical results. *Proceedings of the Lunar and Planetary Science Conference* (Vol. 20, 3–12).

De Maria, G., Balducci, G., Guido, M., & Piacente, V. (1971). Mass spectrometric investigation of the vaporization process of Apollo 12 lunar samples. *Proceedings of the Lunar and Planetary Science Conference* (Vol. 2, 1367–1380).

Dottin, J. W., Kim, S.-T., Wing, B., Farquhar, J., & Shearer, C. (2023). Anomalous ^{33}S in the lunar mantle. *Journal of Geophysical Research: Planets*, *128*(2), e2022JE007597. https://doi.org/10.1029/2022JE007597

Hauri, E. H., Saal, A. E., Rutherford, M. J., & Van Orman, J. A. (2015). Water in the Moon's interior: Truth and consequences. *Earth and Planetary Science Letters*, *409*, 252–264. https://doi.org/10.1016/j.epsl.2014.10.053

Hauri, E. H., Weinreich, T., Saal, A. E., Rutherford, M. C., & Van Orman, J. A. (2011). High pre-eruptive water contents preserved in lunar melt inclusions. *Science*, *333*(6039), 213–215. https://doi.org/10.1126/science.1204626

Head, J. W., Wilson, L., Deutsch, A. N., Rutherford, M. J., & Saal, A. E. (2020). Volcanically induced transient atmospheres on the moon: Assessment of duration, significance, and contributions to polar volatile traps. *Geophysical Research Letters*, *47*(18), e2020GL089509. https://doi.org/10.1029/2020GL089509

Head, J. W., Wilson, L., Hiesinger, H., Van Der Bogert, C., Chen, Y., Dickson, J. L., et al. (2023). Lunar mare basaltic volcanism: Volcanic features and emplacement processes. *Reviews in Mineralogy and Geochemistry*, *89*(1), 453–507. https://doi.org/10.2138/rmg.2023.89.11

Heiken, G. H., McKay, D. S., & Brown, R. W. (1974). Lunar deposits of possible pyroclastic origin. *Geochimica et Cosmochimica Acta*, *38*(11), 1703–1704. https://doi.org/10.1016/0016-7037(74)90187-2

Hui, H., Hess, K.-U., Zhang, Y., Nichols, A. R. L., Peslier, A. H., Lange, R. A., et al. (2018). Cooling rates of lunar orange glass beads. *Earth and Planetary Science Letters*, *503*, 88–94. https://doi.org/10.1016/j.epsl.2018.09.019

Huneke, J. (1978). ^{40}Ar-^{39}Ar microanalysis of single 74220 glass balls and 72435 breccia clasts. *Proceedings of the Lunar and Planetary Science Conference* (Vol. 9, 2345–2362).

Huneke, J., Jessberger, E., Podosek, F., & Wasserburg, G. (1973). ^{40}Ar/^{39}Ar measurements in Apollo 16 and 17 samples and the chronology of metamorphic and volcanic activity in the Taurus-Littrow region. *Proceedings of the Lunar and Planetary Science Conference* (Vol. 4, 1725–1756).

Kurat, G., & Keil, K. (1972). Effects of vaporization and condensation on Apollo 11 glass spherules: Implications for cooling rates. *Earth and Planetary Science Letters*, *14*(1), 7–13. https://doi.org/10.1016/0012-821X(72)90071-4

Liu, Y., & Ma, C. (2022). Direct evidence of volcanic outgassing of Na and K on the Moon from Apollo orange beads. *Icarus*, *382*, 115044. https://doi.org/10.1016/j.icarus.2022.115044

Liu, Y., & Ma, C. (2024). Vapor condensates on the most pristine black beads from a clod in Apollo drive tube 73001: Discovery of lunar NaCl nanocrystals. *Journal of Geophysical Research: Planets*, *129*(10), e2024JE008444. https://doi.org/10.1029/2024JE008444

Liu, Y., Ma, C., & Housley, R. (2020). Contrasting volcanic gases between pyroclastic eruptions on the Moon. *Proceedings of the Lunar and Planetary Science Conference* (Vol. 51, 1166).

Lowry, R. K., Henderson, P., & Nolan, J. (1982). Tracer diffusion of some alkali, Alkaline-earth and transition element ions in a basaltic and an andesitic melt, and the implications concerning melt structure. *Contributions to Mineralogy and Petrology*, *80*(3), 254–261. https://doi.org/10.1007/BF00371355

Ma, C., & Liu, Y. (2019). Discovery of a zinc-rich mineral on the surface of lunar orange pyroclastic beads. *American Mineralogist*, *104*(3), 447–452. https://doi.org/10.2138/am-2019-6896

Meyer, C., McKay, D. S., Anderson, D. H., & Butler, P. (1975). The source of sublimates on the Apollo 15 green and Apollo 17 orange glass samples. *Proceedings of the Lunar and Planetary Science Conference* (Vol. 6, 1673–1699).

Needham, D. H., & Kring, D. A. (2017). Lunar volcanism produced a transient atmosphere around the ancient Moon. *Earth and Planetary Science Letters*, *478*, 175–178. https://doi.org/10.1016/j.epsl.2017.09.002

Ni, P., & Zhang, Y. (2016). Cu diffusion in a basaltic melt. *American Mineralogist*, *101*(6), 1474–1482. https://doi.org/10.2138/am-2016-5544

Ni, P., Zhang, Y., Chen, S., & Gagnon, J. (2019). A melt inclusion study on volatile abundances in the lunar mantle. *Geochimica et Cosmochimica Acta*, *249*, 17–41. https://doi.org/10.1016/j.gca.2018.12.034

Ni, P., Zhang, Y., & Guan, Y. (2017). Volatile loss during homogenization of lunar melt inclusions. *Earth and Planetary Science Letters*, *478*, 214–224. https://doi.org/10.1016/j.epsl.2017.09.010

Ni, P., Zhang, Y., Simon, A., & Gagnon, J. (2017). Cu and Fe diffusion in rhyolitic melts during chalcocite "dissolution": Implications for porphyry ore deposits and tektites. *American Mineralogist*, *102*(6), 1287–1301. https://doi.org/10.2138/am-2017-5885

Pang, R., Yang, J., Li, R., Liu, S., Li, Q., Zhu, D., et al. (2024). Redox condition changes caused by impacts: Insights from Chang'e-5 lunar glass beads. *Science Bulletin*, *69*(10), 1495–1505. https://doi.org/10.1016/j.scib.2024.03.004

Podosek, F., & Huneke, J. (1973). Argon in Apollo 15 green glass spherules (15426): 40Ar39Ar age and trapped argon. *Earth and Planetary Science Letters*, *19*(4), 413–421. https://doi.org/10.1016/0012-821X(73)90184-2

Renggli, C. J., King, P. L., Henley, R. W., & Norman, M. D. (2017). Volcanic gas composition, metal dispersion and deposition during explosive volcanic eruptions on the Moon. *Geochimica et Cosmochimica Acta*, *206*, 296–311. https://doi.org/10.1016/j.gca.2017.03.012

Ross, D. K., Thomas-Keprta, K., Rahman, Z., Wentworth, S., & McKay, D. (2011). FE-SEM, FIB and TEM study of surface deposits of Apollo 15 green glass volcanic spherules. *Proceedings of the Lunar and Planetary Science Conference*, *42*, 2203.

Saal, A. E., Hauri, E. H., Cascio, M. L., Van Orman, J. A., Rutherford, M. C., & Cooper, R. F. (2008). Volatile content of lunar volcanic glasses and the presence of water in the Moon's interior. *Nature*, *454*(7201), 192–195. https://doi.org/10.1038/nature07047

Saunderson, H. C. (2008). Equations of motion and ballistic paths of volcanic ejecta. *Computers and Geosciences*, *34*(7), 802–814. https://doi.org/10.1016/j.cageo.2007.10.004

Shearer, C. K., & Papike, J. J. (1993). Basaltic magmatism on the moon: A perspective from volcanic Picritic glass beads. *Geochimica et Cosmochimica Acta*, *57*(19), 4785–4812. https://doi.org/10.1016/0016-7037(93)90200-G

Spangler, R., Warasila, R., & Delano, J. (1984). 39AR-40Ar ages for the Apollo 15 green and yellow volcanic glasses. *Journal of Geophysical Research*, *89*(S02), B487–B497. https://doi.org/10.1029/JB089iS02p0B487

Strycker, P. D., Chanover, N. J., Miller, C., Hamilton, R. T., Hermalyn, B., Suggs, R. M., & Sussman, M. (2013). Characterization of the LCROSS impact plume from a ground-based imaging detection. *Nature Communications*, *4*(1), 2620. https://doi.org/10.1038/ncomms3620

Su, X., & Zhang, Y. (2024). Volatiles in melt inclusions from lunar mare basalts: Bridging the gap in the H_2O/Ce ratio between melt Inclusions in lunar pyroclastic sample 74220 and other mare samples. *Geochimica et Cosmochimica Acta*, *373*, 232–244. https://doi.org/10.1016/j.gca.2024.04.002

Su, X., Zhang, Y., & Liu, Y. (2025). Sulfur outgassing and in-gassing in lunar orange glass beads and implications for ^{33}S "Anomaly" in the Moon. *Geochimica et Cosmochimica Acta*, *397*, 164–175. https://doi.org/10.1016/j.gca.2025.03.026

Su, X., Zhang, Y., Liu, Y., & Holder, R. M. (2023). Outgassing and in-gassing of Na, K and Cu in lunar 74220 orange glass beads. *Earth and Planetary Science Letters*, *602*, 117924. https://doi.org/10.1016/j.epsl.2022.117924

Su, X., Zhang, Y., Liu, Y., & Holder, R. M. (2025). Data of the paper cooling history and evolution dynamics of green glass beads during lunar fire-fountain eruptions: Insights from Na, K and Cu distributions [Dataset]. *University of Michigan - Deep Blue Data*. https://doi.org/10.7302/caac-5s68

Van Elteren, J. T., Šelih, V. S., & Šala, M. (2019). Insights into the selection of 2D LA-ICP-MS (multi) elemental mapping conditions. *Journal of Analytical Atomic Spectrometry*, *34*(9), 1919–1931. https://doi.org/10.1039/C9JA00166B

Wendt, I., & Carl, C. (1991). The statistical distribution of the mean squared weighted deviation. *Chemical Geology: Isotope Geoscience section*, *86*(4), 275–285. https://doi.org/10.1016/0168-9622(91)90010-T

Williams, T. A., Parman, S. W., Saal, A. E., Akey, A. J., Gardener, J. A., & Ogliore, R. C. (2025). Lunar volcanic gas cloud chemistry: Constraints from glass bead surface sublimates. *Icarus*, *438*, 116607. https://doi.org/10.1016/j.icarus.2025.116607

Zhang, Y. (2008). *Geochemical kinetics*. Princeton University Press.

Zhang, Y., & Gan, T. (2022). Diffusion in melts and magmas. *Reviews in Mineralogy and Geochemistry*, *87*(1), 283–337. https://doi.org/10.2138/rmg.2022.87.07